

Title	Defect termination on crystalline silicon surfaces by hydrogen for improvement in the passivation quality of catalytic chemical vapor-deposited SiN <sub>x</sub> and SiN <sub>x</sub> /P catalytic-doped layers
Author(s)	Thi, Trinh Cham; Koyama, Koichi; Ohdaira, Keisuke; Matsumura, Hideki
Citation	Japanese Journal of Applied Physics, 55(2S): 02BF09-1-02BF09-6
Issue Date	2016-01-22
Type	Journal Article
Text version	author
URL	<a href="http://hdl.handle.net/10119/13833">http://hdl.handle.net/10119/13833</a>
Rights	This is the author's version of the work. It is posted here by permission of The Japan Society of Applied Physics. Copyright (C) 2016 The Japan Society of Applied Physics. Trinh Cham Thi, Koichi Koyama, Keisuke Ohdaira, and Hideki Matsumura, Japanese Journal of Applied Physics, 55(2S), 2016, 02BF09-1-02BF09-6. <a href="http://dx.doi.org/10.7567/JJAP.55.02BF09">http://dx.doi.org/10.7567/JJAP.55.02BF09</a>
Description	

**Defect termination on crystalline silicon surfaces by hydrogen for improvement in the passivation quality of catalytic chemical vapor-deposited SiN<sub>x</sub> and SiN<sub>x</sub>/P catalytic-doped layers**

Trinh Cham Thi<sup>1,2,†</sup>, Koichi Koyama<sup>1,2</sup>, Keisuke Ohdaira<sup>1,2,\*</sup>, and Hideki Matsumura<sup>1,2</sup>

<sup>1</sup>Japan Advanced Institute of Science and Technology (JAIST),

Nomi, Ishikawa 923-1292, Japan

<sup>2</sup>CREST, Japan Science and Technology Agency (JST),

Kawaguchi, Saitama 332-0012, Japan

E-mail: ohdaira@jaist.ac.jp

We investigate the role of hydrogen (H) in the improvement in the passivation quality of silicon nitride (SiN<sub>x</sub>) prepared by catalytic chemical vapor deposition (Cat-CVD) and Cat-CVD SiN<sub>x</sub>/phosphorus (P) Cat-doped layers on crystalline silicon (c-Si) by annealing. Both structures show promising passivation capabilities for c-Si with extremely low surface recombination velocity (SRV) on n-type c-Si. Defect termination by H is evaluated on the basis of defect density ( $N_d$ ) determined by electron spin resonance (ESR) spectroscopy and interface state density ( $D_{it}$ ) calculated by the Terman method. The two parameters are found to be drastically decreased by annealing after SiN<sub>x</sub> deposition. The calculated average  $D_{it}$  at midgap ( $D_{it-average}$ ) is  $2.2 \times 10^{11} \text{ eV}^{-1} \text{ cm}^{-2}$  for the SiN<sub>x</sub>/P Cat-doped c-Si sample with a SRV of 2 cm/s, which is equivalent to

$3.1 \times 10^{11} \text{ eV}^{-1} \text{ cm}^{-2}$  for the  $\text{SiN}_x/\text{c-Si}$  sample with a SRV of 5 cm/s after annealing. The results indicate that H atoms play a critical role in the reduction in  $D_{it}$  for  $\text{SiN}_x/\text{c-Si}$  and  $\text{SiN}_x/\text{P}$  Cat-doped c-Si, resulting in a drastic reduction in SRV by annealing.

<sup>†</sup>Present address: Graduate School of Engineering, Nagoya University, Nagoya 464-8603, Japan

## 1. Introduction

Passivation layers for crystalline silicon (c-Si) have recently been the focus of much attention owing to their important contribution to the improvement in c-Si solar cell efficiency by the reduction in electrical loss caused by defects at the c-Si surface. Besides high passivation quality, passivation films with high transparency and antireflective properties are more preferable. Silicon nitride ( $\text{SiN}_x$ ), amorphous silicon (a-Si),  $\text{Al}_2\text{O}_3$ ,  $\text{SiO}_2$ , and their stacked layers are excellent passivation layers that demonstrate outstanding passivation quality [1-7]. The passivation of these layers relies on defect termination and/or field-effect passivation. Regarding the defect termination mechanism, the surface recombination of minority carriers is suppressed by the reduction in interface state density ( $D_{it}$ ), whereas minority carrier recombination probability is decreased by band bending in field-effect passivation. It has been reported that  $\text{Al}_2\text{O}_3$  films prepared by atomic layer deposition show low surface recombination velocities (SRVs) of 2 and 6 cm/s on 1.9  $\Omega\text{cm}$  floating zone (FZ) n-type c-Si and 1.5  $\Omega\text{cm}$  FZ p-type c-Si, respectively [4]. However,  $\text{Al}_2\text{O}_3$  films do not exhibit antireflective properties on c-Si owing to the mismatch of refractive index.  $\text{SiO}_2$  has high passivation quality, and a low SRV of 2.4 cm/s can be obtained for c-Si passivated with  $\text{SiO}_2$  films formed by thermal oxidation [3]. However, thermal oxidation requires a high temperature ( $>1000$  °C), which is not suitable particularly for the fabrication of silicon heterojunction solar cells containing a-Si films with low thermal tolerance. Among these passivation layers, stoichiometric  $\text{SiN}_x$  films with a refractive index of  $\sim 2$  is the most promising passivation layer because they show not only excellent passivation quality and high transparency but also significant antireflective properties on c-Si. Moreover, the preparation of  $\text{SiN}_x$  films does not require a high temperature. A

conventional method used to fabricate SiN<sub>x</sub> films is plasma-enhanced chemical vapor deposition (PECVD). PECVD SiN<sub>x</sub> films with high passivation quality having SRVs of 2-10 cm/s have been reported [4,5,7]. The passivation mechanism of PECVD SiN<sub>x</sub> layers is mainly based on field-effect passivation originating from positive fixed charges in the SiN<sub>x</sub> films, whereas thermally grown SiO<sub>2</sub> layers can significantly reduce  $D_{it}$ . Typical values of  $D_{it}$  and fixed charge density ( $Q_f$ ) are  $\sim 10^{10}$  eV<sup>-1</sup>cm<sup>-2</sup> and  $\sim 10^{10}$  cm<sup>-2</sup> for SiO<sub>2</sub> and  $\sim 10^{11}$  eV<sup>-1</sup>cm<sup>-2</sup> and  $\sim 10^{11}$  cm<sup>-2</sup> for PECVD SiN<sub>x</sub> layers, respectively [8]. Ion bombardment during PECVD tends to deteriorate film/interface quality, and if this problem can be solved, SiN<sub>x</sub> films with higher passivation quality will be realized.

Catalytic CVD (Cat-CVD), often also referred to as hot-wire CVD, is one of the potential methods to overcome the drawback of PECVD [9,10]. Radical species are formed by the decomposition of source gas molecules on a heated catalyzing wire in Cat-CVD. c-Si surfaces are thus not exposed to energetic ions, and good film/c-Si interface properties can be realized. Moreover, the H content of Cat-CVD films is lower than that of PECVD films, resulting in higher stability against light exposure [10]. The Cat-CVD system can also be utilized to form ultrathin doping layers by exposing c-Si surfaces to radicals formed by the decomposition of PH<sub>3</sub> or B<sub>2</sub>H<sub>6</sub> radicals [11-15]. This doping technique, catalytic doping (Cat-doping), can be applied to the improvement in passivation quality since the thin doping layers formed act as field-effect passivation layers. Single Cat-CVD SiN<sub>x</sub> and Cat-CVD SiN<sub>x</sub>/phosphorus (P) Cat-doped layer structures can be promising candidates as passivation layers for c-Si. In our previous studies, extremely low  $SRV_{max}$  values of 5 and 2 cm/s have been demonstrated for n-type c-Si passivated with Cat-CVD SiN<sub>x</sub> and Cat-CVD SiN<sub>x</sub>/P Cat-doped layer structures, respectively [13,16]. The SiN<sub>x</sub> films used in this study have been confirmed

to have high transparency and good antireflective properties [16]. It should be emphasized that these extremely low  $SRV_{max}$  values can be obtained only after postannealing at an appropriate temperature [13,16]. For a Cat-CVD  $SiN_x/c$ -Si sample, the significant reduction in SRV by postannealing is supposed to be due to defect termination by hydrogen atoms. For a sample with a P Cat-doped layer, the drastic reduction in SRV is probably due to field-effect passivation induced by P donors and defect termination by H during annealing.

In this study, to quantitatively clarify the role of H in the defect termination effect on the passivation of c-Si surfaces, we focus on the following topics: the etching effect of H atoms on c-Si surfaces during the deposition process, H distribution in the films, defect density ( $N_d$ ) in  $SiN_x$  films, and  $D_{it}$  at Cat-CVD  $SiN_x/c$ -Si and  $SiN_x/P$  Cat-doped c-Si interfaces. The results show that  $N_d$  and  $D_{it}$  at midgap ( $D_{it-average}$ ) decrease significantly after annealing.  $D_{it-average}$  drastically decreases from  $2 \times 10^{12}$  to  $3 \times 10^{11}$   $eV^{-1}cm^{-2}$  after annealing. For a sample with a P Cat-doped layer,  $D_{it-average}$  also effectively decreases from  $2 \times 10^{12}$  to  $2 \times 10^{11}$   $eV^{-1}cm^{-2}$  after annealing. The results obtained indicate that H atoms terminate dangling bonds at film/c-Si interfaces. The slightly smaller  $D_{it-average}$  for the sample with a P Cat-doped layer may be the contribution of H atoms in a P Cat-doped layer.

## 2. Experimental procedure

To clarify the effect of H on the passivation mechanism, we firstly examined the effect of etching by H atoms on c-Si surfaces during  $SiN_x$  deposition. A 290- $\mu m$ -thick n-type (100) FZ Si wafer with a resistivity of 2.5  $\Omega cm$  was cleaned in 5% hydrofluoric acid (HF) diluted with deionized (DI) water for 10 s to remove native oxides. The

sample was then passivated with SiN<sub>x</sub> films deposited by Cat-CVD under conditions shown in Table I. After that, the SiN<sub>x</sub> films were removed in 30% HF diluted with DI water for 5 s. The complete removal of the SiN<sub>x</sub> films was confirmed using the Cauchy model of a spectroscopic ellipsometer (J. A. Woollam WVASE32) for data analysis [17]. Surface morphology was then observed by atomic force microscopy (AFM). The surface morphology of bare c-Si after dipping in 30% HF for 5 s was also measured for comparison. For this measurement, two SiN<sub>x</sub> deposition conditions were selected. Under one condition, a SiN<sub>x</sub> film was deposited at a substrate temperature ( $T_s$ ) of 100 °C, at which the most significant improvement in the passivation quality of SiN<sub>x</sub> by annealing is achieved. Under the other condition, SiN<sub>x</sub> films were deposited at a  $T_s$  of 300 °C, at which the highest effective minority carrier lifetime ( $\tau_{eff}$ ) is obtained for an as-deposited sample. The surface morphology of the samples was observed immediately after dipping in DI water and drying with a N<sub>2</sub> gun. H distribution is one of the important factors considered to investigate the passivation mechanism of H in SiN<sub>x</sub> films. In this study, the H profiles in SiN<sub>x</sub> films before and after annealing at 350 °C for 30 min were measured by secondary ion mass spectrometry (SIMS). We evaluated  $N_d$  using five 2.5×20 mm<sup>2</sup> quartz glass substrates with 100-nm-thick SiN<sub>x</sub> films for each substrate (500 nm in total) by electron spin resonance (ESR) spectroscopy (JEOL JES-FA100) at room temperature. For  $\tau_{eff}$  measurement, both surfaces of 290- $\mu$ m-thick n-type (100) FZ Si wafers with a resistivity of 2.5  $\Omega$ cm were passivated with SiN<sub>x</sub> layers. We carried out microwave photoconductivity decay ( $\mu$ -PCD) measurement (KOBELCO LTA-1510EP) using a pulse laser with a wavelength of 904 nm and a photon density of  $5 \times 10^{13}$  cm<sup>-2</sup>.  $\tau_{eff}$  is expressed as

$$\frac{1}{\tau_{eff}} = \frac{1}{\tau_{bulk}} + \frac{2S}{W},$$

where  $\tau_{bulk}$ ,  $W$ , and  $S$  represent the minority carrier lifetime in c-Si bulk, wafer thickness, and SRV, respectively. In this study, we calculated the maximum SRV ( $SRV_{max}$ ) by assuming  $\tau_{bulk}=\infty$ .

In order to accurately confirm defect termination by H atoms on c-Si surfaces, we calculated  $D_{it}$  from the high-frequency experimental capacitance-voltage (C-V) curves obtained from metal-insulator-semiconductor (MIS) structures by the Terman method [18,19]. A cross-sectional schematic view of the MIS structure is shown in Fig. 1. The experimental preparation for the sample structure has been described elsewhere [16]. The deposition conditions of  $SiN_x$  films are the same as in Ref. 16 and are summarized in Table I. For a sample with P Cat doping, we used the same condition as that under which we obtained the best SRV after annealing, as reported in Ref. 13. The P Cat doping conditions are summarized in Table II. The samples were annealed three times. The first annealing was conducted after P doping at 400 °C for 30 min, and the second annealing was conducted after  $SiN_x$  film deposition at 350 °C for 30 min. An Al ohmic contact is formed on the back side of the samples by evaporation and annealing at 400 °C for 10 min. Finally, the front Al electrode was evaporated. A  $SiN_x$ /P Cat-doped layer/c-Si sample for lifetime measurement was also prepared and annealed by the same procedure to confirm high passivation quality. The Terman method is mainly based on the comparison of the shapes of the theoretical C-V curve and experimental high-frequency C-V curve. In this study, a high frequency of 1 MHz was used for C-V measurement. C-V curves were measured using a Keithley 6517A electrometer/high resistance meter and a 6440B component analyzer. The theoretical curve was calculated



using the equations shown in Ref. 18.  $D_{it}$  as a function of surface potential is calculated using the following equation [19]:

$$D_{it} = \frac{d(V_{g\_measured} - V_{g\_theoretical}) C_i}{d\psi_s} \frac{C_i}{q},$$

where  $V_g$  is the applied voltage,  $C_i$  is the insulator capacitance,  $q$  is the elementary charge, and  $\psi_s$  is the surface potential.

### 3. Results and discussion

#### 3.1. H etching during $SiN_x$ deposition

Cat-CVD is a well-known method, which causes no plasma-induced damage to the substrate surface. However, the substrate surface may be etched by H atoms when it is exposed to a high density of H atoms at a  $T_s$  lower than 150 °C [20]. In our study, the lowest  $SRV_{max}$  of 5 cm/s was achieved for c-Si passivated with  $SiN_x$  films deposited at a  $T_s$  of 100 °C after annealing. All the samples showed high  $SRV_{max}$  values ( $\geq 30$  cm/s) before annealing [16]. One possible reason is supposed to be H etching during  $SiN_x$  deposition. However, since the  $SiN_x$  deposition rate of ~30 nm/min at a  $T_s$  of 100 °C is sufficiently high, the rapid coverage of the c-Si surface by  $SiN_x$  may suppress the effect of H etching. To obtain experimental evidence for this speculation, we investigated the effect of H etching during  $SiN_x$  film deposition by evaluating the surface morphology of c-Si after the deposition and removal of  $SiN_x$  films. We firstly deposited  $SiN_x$  films on the c-Si surface and then examined the surface morphology of the sample after removing the  $SiN_x$  films using HF solution. The thickness and refractive index of the  $SiN_x$  films were 80 nm and ~2.0, respectively; however, no such films were observed at

all by spectroscopic ellipsometry after HF dipping. This observation indicates that  $\text{SiN}_x$  was completely removed from c-Si surfaces.

Figure 2 shows the AFM images of c-Si surfaces after the removal of the  $\text{SiN}_x$  films. The morphology of the c-Si surface without  $\text{SiN}_x$  deposition after dipping in HF is also shown for comparison. For the sample without  $\text{SiN}_x$  film deposition, the root-mean-square roughness ( $R_{rms}$ ) of the c-Si surface is 0.095 nm, whereas those of the samples with  $\text{SiN}_x$  deposition at  $T_s$  values of 100 and 300 °C are 0.13 and 0.10 nm, respectively. The  $R_{rms}$  of the bare c-Si surface dipped in HF solution is comparable to those of the samples without HF etching, as reported in Ref. 13. This suggests that the c-Si surface does not deteriorate after dipping in 30% HF for 5 s. The slightly higher  $R_{rms}$  values obtained for the samples with  $\text{SiN}_x$  deposition and removal indicate that etching occurs during  $\text{SiN}_x$  deposition. The  $R_{rms}$  of the sample with a  $\text{SiN}_x$  film deposited at 300 °C is lower than that of the sample with a  $\text{SiN}_x$  film deposited at 100 °C. H etching during  $\text{SiN}_x$  film deposition might therefore be a possible reason for the higher  $\tau_{\text{eff}}$  of an as-deposited  $\text{SiN}_x/\text{c-Si}$  structure with  $\text{SiN}_x$  deposited at a higher  $T_s$ . However, since a low  $SRV_{\text{max}}$  of 5 cm/s is obtained for the  $\text{SiN}_x/\text{c-Si}$  structure with  $\text{SiN}_x$  films deposited at a  $T_s$  of 100 °C, the effect of etching by atomic hydrogen during  $\text{SiN}_x$  deposition on passivation quality may be negligible.

### ***3.2. H distributions in $\text{SiN}_x$ films before and after annealing***

The improvement in the passivation quality of  $\text{SiN}_x$  films by annealing has been reported by many groups [21-23]. The H distribution in  $\text{SiN}_x$  films is one of the key factors affecting the termination of defects on c-Si surfaces by H atoms during

annealing. The distribution of H atoms inside  $\text{SiN}_x$  films can provide information on H diffusion or release to the environment during annealing, which may lead to the profound understanding of the H defect termination mechanism. In our previous report, H content was calculated from Fourier-transform infrared (FT-IR) spectra using the Lanford method [16, 24]. We found that the Si-H bonding peak signal intensity slightly increases after annealing. The integrated intensity of the Si-H bonding peak signal increases by ~10% after annealing, whereas no change in that of the N-H bonding peak signal is observed. This suggests that H atoms terminate the Si dangling bond inside c-Si and also at the  $\text{SiN}_x/\text{c-Si}$  interface during annealing. We also supposed that H atoms diffuse into the  $\text{SiN}_x/\text{c-Si}$  interface, and that more dangling bonds are terminated during annealing [16].

Figure 3 shows the SIMS profiles of H concentration in  $\text{SiN}_x$  films deposited at a  $T_s$  of 100 °C before and after annealing at 350 °C for 30 min. The H concentration is constant with the depth of  $\text{SiN}_x$  films. One can see in Fig. 3 that there is no significant difference in H concentration between the samples before and after annealing. Note that the H concentration calculated from the FT-IR spectra of the samples is based on Si-H and N-H bonds in  $\text{SiN}_x$  films. The integrated intensity of the Si-H bonding peak signal increases when the  $\text{SiN}_x$  films are annealed at 350 °C. The SIMS profiles suggest that not diffusion but bonding rearrangement during annealing contributes to defect termination, resulting in the improvement in passivation quality. A possible mechanism is that H atoms existing in voids inside  $\text{SiN}_x$  and at the  $\text{SiN}_x/\text{c-Si}$  interface recombine with neighboring Si dangling bonds. In order to confirm defect termination by annealing, in the next subsection, we will report on  $N_d$  in  $\text{SiN}_x$  films and  $D_{it}$  at the  $\text{SiN}_x/\text{c-Si}$  interfaces.

### 3.3. $N_d$ in $\text{SiN}_x$ films and $D_{it}$ at $\text{SiN}_x/c\text{-Si}$ interfaces

Si dangling bonds back-bonded to three N atoms,  $\text{N}_3\equiv\text{Si}\cdot$ , generally called K centers, are the main dangling bonds in  $\text{SiN}_x$  films. A K center has three states:  $\text{K}^0$ ,  $\text{K}^-$ , and  $\text{K}^+$  [25-32].  $\text{K}^+$  is the origin of fixed charges in  $\text{SiN}_x$  films and is easily determined by the negative shift of C-V curves [29-32].  $\text{K}^0$  is a dangling bond containing an unpaired electron and is observable by ESR spectroscopy [25-28]. We have reported that both  $\text{K}^0$ , corresponding to  $N_d$ , and  $\text{K}^+$ , corresponding to  $Q_f$ , decrease markedly after annealing [16]. In particular, for a  $\text{SiN}_x$  film deposited at a  $T_s$  of 100 °C,  $Q_f$  decreases from  $1\times 10^{12}$  to  $7\times 10^{11}$   $\text{cm}^{-2}$  and  $N_d$  decreases from  $2\times 10^{18}$  to  $4\times 10^{17}$   $\text{cm}^{-3}$  after annealing. Figure 4 shows the ESR spectra of  $\text{SiN}_x$  films deposited at various  $T_s$  values before and after annealing at 350 °C for 30 min. The g values obtained were 2.0033-2.0047 for  $\text{SiN}_x$  films deposited at various  $T_s$  values, and the films deposited at lower  $T_s$  values resulted in higher g values. The g reported for the  $\text{K}^0$  defects is 2.003 [25], and that for Si dangling bonds in a-Si is 2.0055 [33]. The g value of  $\text{SiN}_x$  films must thus depend on the chemical composition of the films. The g values obtained in this study may imply that the  $\text{SiN}_x$  films formed are slightly Si-rich, particularly for those formed at lower  $T_s$  values. This is reasonable because the  $\text{SiN}_x$  films are formed so that their refractive indices become 2 and the films formed at lower  $T_s$  values have lower densities. From Fig. 4, one can see that the intensities of dangling bond peak signals decrease greatly after annealing. This is clear evidence of defect termination by H in  $\text{SiN}_x$  films during annealing. This result implies that H can terminate defects not only inside  $\text{SiN}_x$  but also

on a SiN<sub>x</sub>/c-Si interface during annealing, which can lead to a drastic reduction in  $SRV_{max}$  after annealing.

To demonstrate more clearly the effect of defect termination by H atoms at the interface of a SiN<sub>x</sub>/c-Si structure, we estimated the  $D_{it}$  of these samples from their C-V curves by the Terman method. Figure 5 shows the experimental and theoretical C-V curves of the MIS structures with SiN<sub>x</sub> films deposited at a  $T_s$  of 100 °C before and after annealing. The theoretical C-V curves are drawn under the assumption of no  $D_{it}$ . Because positive fixed charges exist in SiN<sub>x</sub> films, the experimental C-V curves were negatively shifted. In the figures, we positively shifted the experimental C-V curves by the flat band voltage values to see clearly the difference between the theoretical and experimental C-V curves. One can see that there is a marked difference in shape between the theoretical and experimental C-V curves of the samples before annealing, whereas a good fitting of the theoretical and experimental curves is obtained for the samples after annealing. This result implies that the samples have higher  $D_{it}$  values before annealing than after annealing. According to the results of analysis by the Terman method, the  $D_{it}$  values of the samples before annealing are on the order of  $10^{12}$  eV<sup>-1</sup>cm<sup>-2</sup>, whereas those of the samples after annealing are on the order of  $10^{11}$  eV<sup>-1</sup>cm<sup>-2</sup>. Figure 6 shows the  $D_{it}$  values of SiN<sub>x</sub>/c-Si structures as a function of surface potential for SiN<sub>x</sub> samples deposited at  $T_s$  values of 70 and 100 °C before and after annealing. A significant decrease in  $D_{it-average}$  is observed for the samples after annealing. This observation is consistent with the improvement in passivation quality and the resulting reduction in SRV. In particular, in the case of the sample deposited at 100 °C, which demonstrates a low  $SRV_{max}$  of 5 cm/s after annealing, the experimental and ideal C-V curves show the best coincidence and the  $D_{it-average}$  calculated is  $3.1 \times 10^{11}$  eV<sup>-1</sup>cm<sup>-2</sup>.

Figure 7 shows the  $SRV_{max}$  values of the  $SiN_x/c-Si$  samples deposited at various  $T_s$  values before and after annealing at 350 °C for 30 min as a function of  $D_{it\_average}$ . For the samples before annealing with large  $SRV_{max}$  values, the  $D_{it\_average}$  values are on the order of  $10^{12}$  eV<sup>-1</sup>cm<sup>-2</sup>.  $D_{it\_average}$  decreases to the order of  $10^{11}$  eV<sup>-1</sup>cm<sup>-2</sup> after annealing, by which a  $SRV_{max}$  lower than 10 cm/s can be obtained. We suppose that the SRVs of the samples after annealing are strongly affected by  $D_{it\_average}$  rather than by  $Q_f$ ; thus,  $SRV_{max}$  increases linearly with  $D_{it\_average}$ . On the other hand, the samples before annealing have higher  $Q_f$  and  $D_{it\_average}$ , and both of the two parameters contribute greatly to the passivation mechanism. The linear tendency of SRV against  $D_{it\_average}$  could thus not be obtained for the samples before annealing. The drastic decrease in  $D_{it}$  after annealing strongly supports the speculation that H atoms terminate defects at a  $SiN_x/c-Si$  interface. The calculated result in our study is in good agreement with previous reports on PECVD  $SiN_x$  films [8,29,34,35]. Wan *et al.* reported the  $D_{it}$  of PECVD  $SiN_x/c-Si$  interfaces estimated by the Terman method [34]. From their report,  $SRV_{max}$  becomes less than 10 cm/s when  $D_{it}$  is on the order of  $10^{10}$  eV<sup>-1</sup>cm<sup>-2</sup> and  $Q_f \sim 10^{11}$  cm<sup>-2</sup>.  $SRV_{max} > 100$  cm/s corresponds to  $D_{it} > 10^{12}$  eV<sup>-1</sup>cm<sup>-2</sup> and  $Q_f \sim 10^{12}$  cm<sup>-2</sup>. These are consistent with  $D_{it}$  and  $SRV_{max}$  obtained in our study. Our Cat-CVD  $SiN_x$  films have  $Q_f > 10^{11}$  cm<sup>-2</sup> even after annealing. The passivation quality of  $SiN_x$  films on c-Si depends on not only  $D_{it}$  but also  $Q_f$ . A  $Q_f$  of  $7 \times 10^{11}$  cm<sup>-2</sup> and a  $D_{it}$  of  $3.1 \times 10^{11}$  eV<sup>-1</sup>cm<sup>-2</sup> are typical values for the lowest  $SRV_{max}$  obtained for c-Si passivated with Cat-CVD  $SiN_x$  films.

### 3.4. $D_{it}$ at $SiN_x/P$ Cat-doped c-Si interface

As reported previously, P Cat doping contributes significantly to the improvement in the passivation quality of SiN<sub>x</sub>/c-Si structures. A significantly low  $SRV_{max}$  of 2 cm/s has been achieved for a SiN<sub>x</sub>/P Cat-doped c-Si structure after annealing [13]. The drastic reduction in  $SRV_{max}$  is supposed to be mainly due to the field effect passivation induced by P donors. The P doping process is conducted at a low  $T_s$  of 80 °C and the sample surface is exposed to a large number of H atoms, and H etching may occur. Etching can increase surface area, generate more dangling bonds, and/or cause insufficient film coverage on the c-Si surface. On the other hand, H inside the P Cat-doped layer may terminate dangling bonds at the interface of SiN<sub>x</sub>/P Cat-doped c-Si and contribute to the reduction in SRV during annealing.

Figure 8 shows the  $D_{it}$  values of SiN<sub>x</sub>/P Cat-doped c-Si and SiN<sub>x</sub>/c-Si samples after annealing at 350 °C for 30 min. The  $D_{it-average}$  of the SiN<sub>x</sub>/P Cat-doped c-Si sample is  $2.0 \times 10^{12}$  eV<sup>-1</sup>cm<sup>-2</sup> before annealing, whereas it decreases to  $2.1 \times 10^{11}$  eV<sup>-1</sup>cm<sup>-2</sup> after annealing. Those values are equivalent to those of the SiN<sub>x</sub>/c-Si sample. We can thus assume that H atoms in a SiN<sub>x</sub> film contribute greatly to defect termination on a c-Si surface even in the case of samples with P Cat-doped layers. The reason for the slightly smaller  $D_{it}$  of the SiN<sub>x</sub>/P Cat-doped c-Si sample than that of the SiN<sub>x</sub>/c-Si sample might be the effect of H atoms contained in a P Cat-doped layer. Taken together, we can conclude that both field effect passivation and H defect termination contribute significantly to the improvement in the passivation quality of SiN<sub>x</sub>/P Cat-doped c-Si structures.

#### 4. Conclusions

H atoms play an important role in the reduction in SRV for both SiN<sub>x</sub>/P Cat-doped c-Si and SiN<sub>x</sub>/c-Si samples. Although the c-Si surface is damaged slightly by H etching during P Cat doping and film deposition, H atoms inside SiN<sub>x</sub> films can terminate a large number of defects at SiN<sub>x</sub>/c-Si interfaces during annealing, resulting in the marked improvement in film passivation quality.  $D_{it-average}$  drastically decreases from  $2 \times 10^{12}$  to  $3 \times 10^{11}$  eV<sup>-1</sup>cm<sup>-2</sup> after annealing in the SiN<sub>x</sub>/c-Si structure. For the sample with a P Cat-doped layer,  $D_{it-average}$  is also effectively reduced from  $2 \times 10^{12}$  to  $2 \times 10^{11}$  eV<sup>-1</sup>cm<sup>-2</sup> by annealing. The low  $D_{it-average}$  obtained indicates the good interface quality of Cat-CVD film/c-Si. The results obtained also demonstrate that H atoms play an important role in the improvement in the passivation quality of SiN<sub>x</sub>/c-Si and SiN<sub>x</sub>/P Cat-doped c-Si structures.

### **Acknowledgement**

We would like to acknowledge the JST CREST program.



## References

- [1] R. Hezel and K. Jaeger, *J. Electrochem. Soc.* **136**, 518 (1989).
- [2] A. Focsa, A. Slaoui, H. Charifi, J. P. Stocquert, and S. Roques, *Mater. Sci. Eng. B* **159-160**, 242 (2009).
- [3] M. J. Kerr and A. Cuevas, *Semicond. Sci. Technol.* **17**, 35 (2002).
- [4] B. Hoex, J. Schmidt, P. Pohl, M. C. M. van de Sanden, and W. M. M. Kessels, *J. Appl. Phys.* **104**, 044903 (2008).
- [5] J. Schmidt and M. Kerr, *Sol. Energy Mater. Sol. Cells* **65**, 585 (2001).
- [6] Y. Larionova, V. Mertens, N. Harder, and R. Brendel, *Appl. Phys. Lett.* **96**, 32105 (2010).
- [7] S. Duttgupta, B. Hoex, and A. G. Aberle, presented at 22nd Int. Photovoltaic Science and Engineering Conf., 2012.
- [8] S. W. Glunz, *Adv. OptoElectron.* **2007**, 2 (2007).
- [9] H. Matsumura, *J. Appl. Phys.* **65**, 4396 (1989).
- [10] R. E. I. Schropp, *ECS Trans.* **25**, 3 (2009)
- [11] H. Matsumura, M. Miyamoto, K. Koyama, and K. Ohdaira, *Sol. Energy Mater. Sol. Cells* **95**, 797 (2011).
- [12] T. Hayakawa, Y. Nakashima, M. Miyamoto, K. Koyama, K. Ohdaira, and H. Matsumura, *Jpn. J. Appl. Phys.* **50**, 121301 (2011).
- [13] T. C. Thi, K. Koyama, K. Ohdaira, and H. Matsumura, *J. Appl. Phys.* **116**, 114502 (2014).
- [14] H. Matsumura, T. Hayakawa, T. Ohta, Y. Nakashima, M. Miyamoto, T. C. Thi, K. Koyama, and K. Ohdaira, *J. Appl. Phys.* **116**, 044510 (2014).
- [15] T. Ohta, K. Koyama, K. Ohdaira, and H. Matsumura, *Thin Solid Films* **575**, 92

(2015).

[16] T. C. Thi, K. Koyama, K. Ohdaira, and H. Matsumura, *Jpn. J. Appl. Phys.* **53**, 022301 (2014).

[17] Guide to Using WVASE32™: Software for Vase and M-44 Ellipsometers (J. A. Woollam, Lincoln, NE, 1989) p. 159.

[18] E. H. Nicollian and J. R. Brews, *MOS Physics and Technology* (Wiley, New York, 1982) 3<sup>rd</sup> ed., pp. 99 and 325.

[19] D. K. Schroder, *Semiconductor Device and Characterization* (Wiley, New York, 2006) p. 351.

[20] H. Matsumura, K. Kamesaki, A. Masuda, and A. Izumi, *Jpn. J. Appl. Phys.* **40**, L289 (2001).

[21] B. Sopori, R. Reedy, K. Jones, Y. Yan, and M. Al-Jassim, *Proc. 31st IEEE Photovoltaic Specialists Conf.*, 2005, p. 1039.

[22] J. Hong, W. M. M. Kessels, M. J. Soppe, A. W. Weeber, W. M. Arnoldbik, and M. C. M. Van de Sanden, *J. Vac. Sci. Technol. B* **21**, 2123 (2003).

[23] V. Yelundur, A. Rohatgi, J. I. Hanoka, and R. Reedy, *Proc. 19th European Photovoltaic Solar Energy Conf.*, 2004, p. 951.

[24] W. A. Lanford, *J. Appl. Phys.* **49**, 2473 (1978).

[25] D. T. Krick, P. M. Lenahan, and J. Kanicki, *J. Appl. Phys.* **64**, 3558 (1988).

[26] P. M. Lenahan, D. T. Krick, and J. Kanicki, *Appl. Surf. Sci.* **39**, 392 (1989).

[27] P. M. Lenahan and S. E. Curry, *Appl. Phys. Lett.* **56**, 157 (1990).

[28] W. L. Warren and P. M. Lenahan, *Phys. Rev. B* **42**, 1773 (1990).

[29] J. -F. Lelièvre, E. Fourmond, A. Kaminski, O. Palais, D. Ballutaud, and M. Lemiti, *Sol. Energy Mater. Sol. Cells* **93**, 1281 (2009).

- [30] L. Xiangna, Z. Zhouyin, and W. Yong, *Chin. Phys. Lett.* **7**, 79 (1990).
- [31] J. Robertson, W. L. Warren, and J. Kanicki, *J. Non-Cryst. Solids* **187**, 297 (1995).
- [32] W. L. Warren, J. Robertson, and J. Kanicki, *Appl. Phys. Lett.* **6**, 2685 (1993).
- [33] R. A. Street, *Hydrogenated Amorphous Silicon*, Solid State Science Series, (Cambridge University Press, Cambridge, U.K., 1991) Cambridge Solid State Science Series, p. 107
- [34] Y. Wan, K. R. McIntosh, and A. F. Thomson, *AIP Adv.* **3**, 032113 (2013).
- [35] S. Duttagupta, F. Lin, M. Wilson, M. B. Boreland, B. Hoex, and A. G. Aberle, *Prog. Photovoltaics* **22**, 641 (2012).

## Figure captions

Fig.1. Cross-sectional schematic view of a sample used for C-V measurement.

Fig. 2. AFM images of c-Si surfaces after removing SiN<sub>x</sub> films. (a) Bare c-Si dipped in 30% HF for 5 s, (b) c-Si after removing a SiN<sub>x</sub> film deposited at a  $T_s$  of 100 °C, and (c) c-Si after removing a SiN<sub>x</sub> film deposited at a  $T_s$  of 300 °C.

Fig. 3. SIMS profiles of H atoms in SiN<sub>x</sub> films deposited at a  $T_s$  of 100 °C before and after annealing at 350 °C for 30 min.

Fig. 4. ESR spectra of SiN<sub>x</sub> films deposited at various  $T_s$  values before and after annealing at 350 °C for 30 min.

Fig. 5. Experimental and theoretical C-V curves of the MIS structures with SiN<sub>x</sub> films deposited at a  $T_s$  value of 100 °C before annealing at 350 °C and after annealing for 30 min.

Fig. 6.  $D_{it}$  values of SiN<sub>x</sub>/c-Si interfaces with SiN<sub>x</sub> films deposited at 70 and 100 °C before annealing at 350 °C and after annealing at 350 °C for 30 min as a function of surface potential.

Fig. 7.  $SRV_{max}$  values of SiN<sub>x</sub>/c-Si samples deposited at various  $T_s$  values before and after annealing at 350 °C for 30 min as a function of  $D_{it-average}$ . Red circles and black square dots represent the values of the samples before and after annealing, respectively.

Fig. 8.  $D_{it}$  values of SiN<sub>x</sub>/P Cat-doped c-Si and SiN<sub>x</sub>/c-Si interfaces after annealing at 350 °C for 30 min as a function of surface potential.

Table I. Deposition conditions of SiN<sub>x</sub> films.

Film	SiH <sub>4</sub> (sccm)	NH <sub>3</sub> (sccm)	Gas pressure (Pa)	T <sub>s</sub> (°C)	T <sub>cat</sub> (°C)	Duration (s)
1	8.7	150	10	50	1800	144
2	8.4	150	10	70	1800	160
3	8	150	10	100	1800	190-210
4	7	150	10	150	1800	220
5	6	150	10	200	1800	240
6	5.3	150	10	300	1800	300

Table II. P Cat doping conditions.

Gas source	He-diluted 2.25% PH <sub>3</sub> 20 sccm
Substrate temperature	90 °C
Pressure	1 Pa
Catalyzer temperature	1300 °C
Exposure duration	60 s

Figure 1.

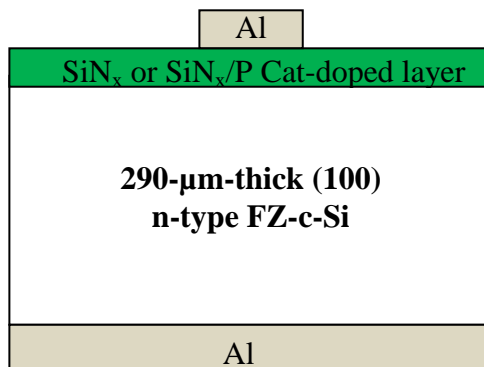


Figure 2.

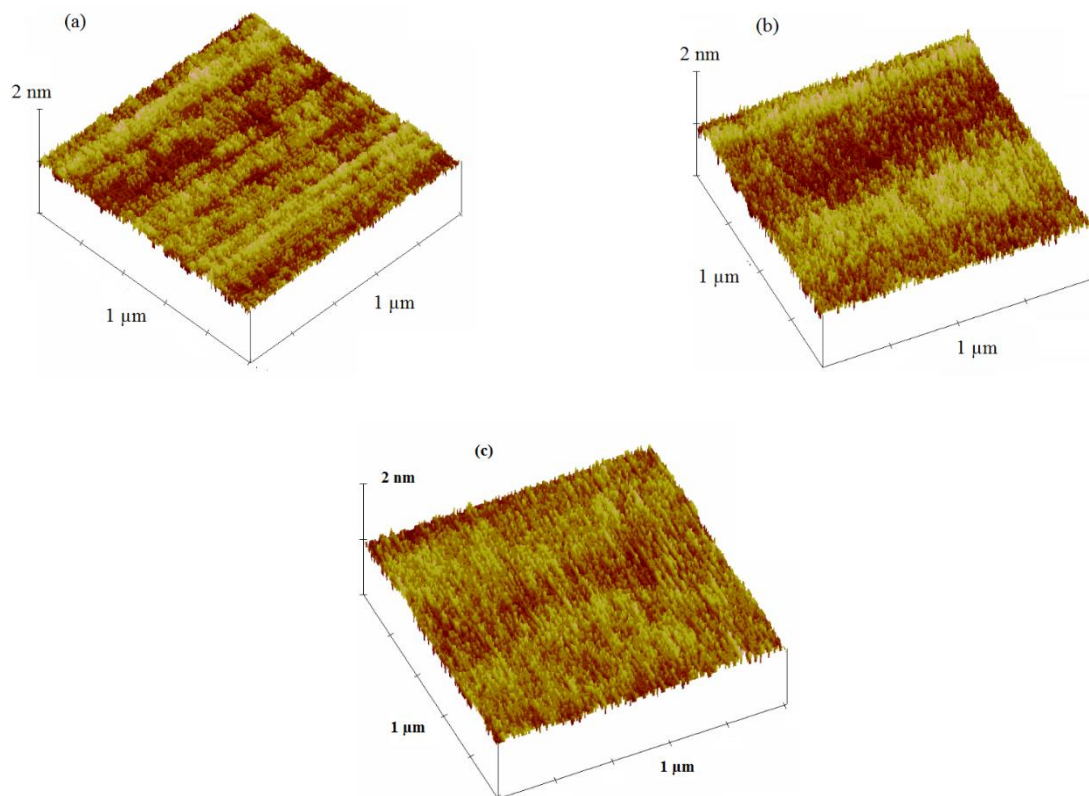


Figure 3

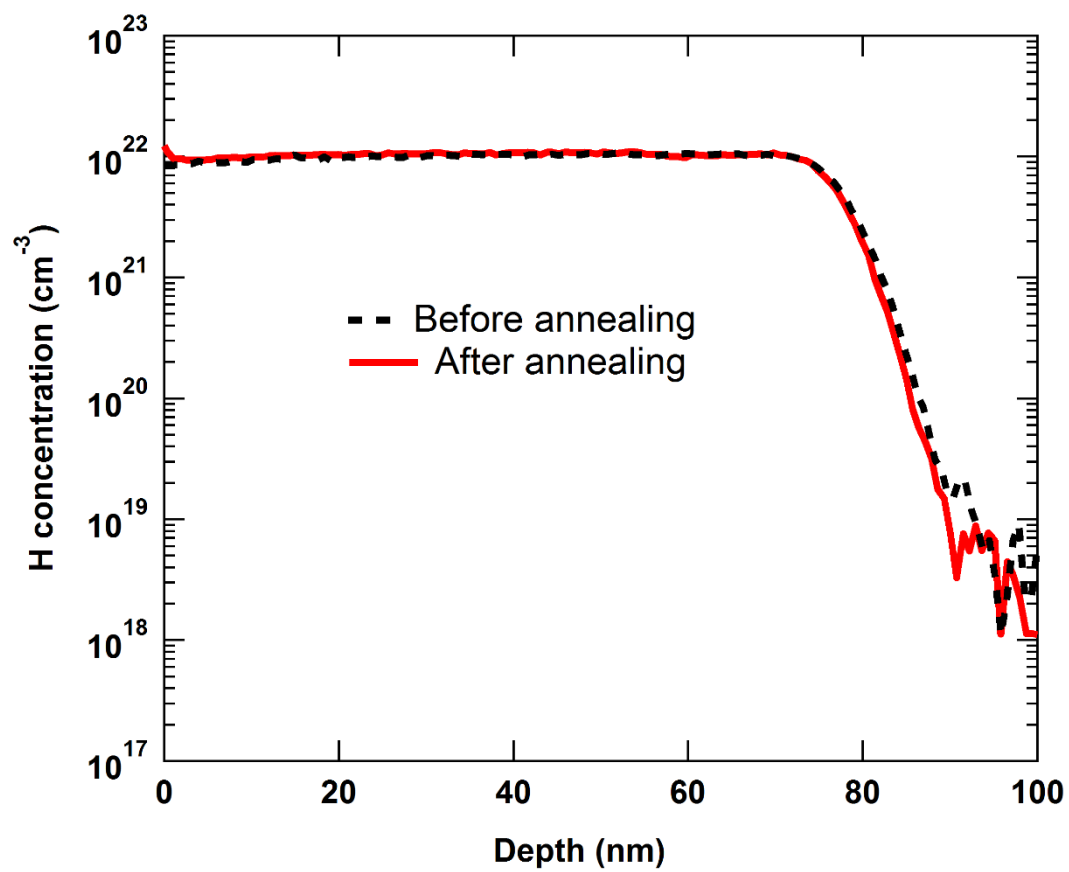




Figure 4

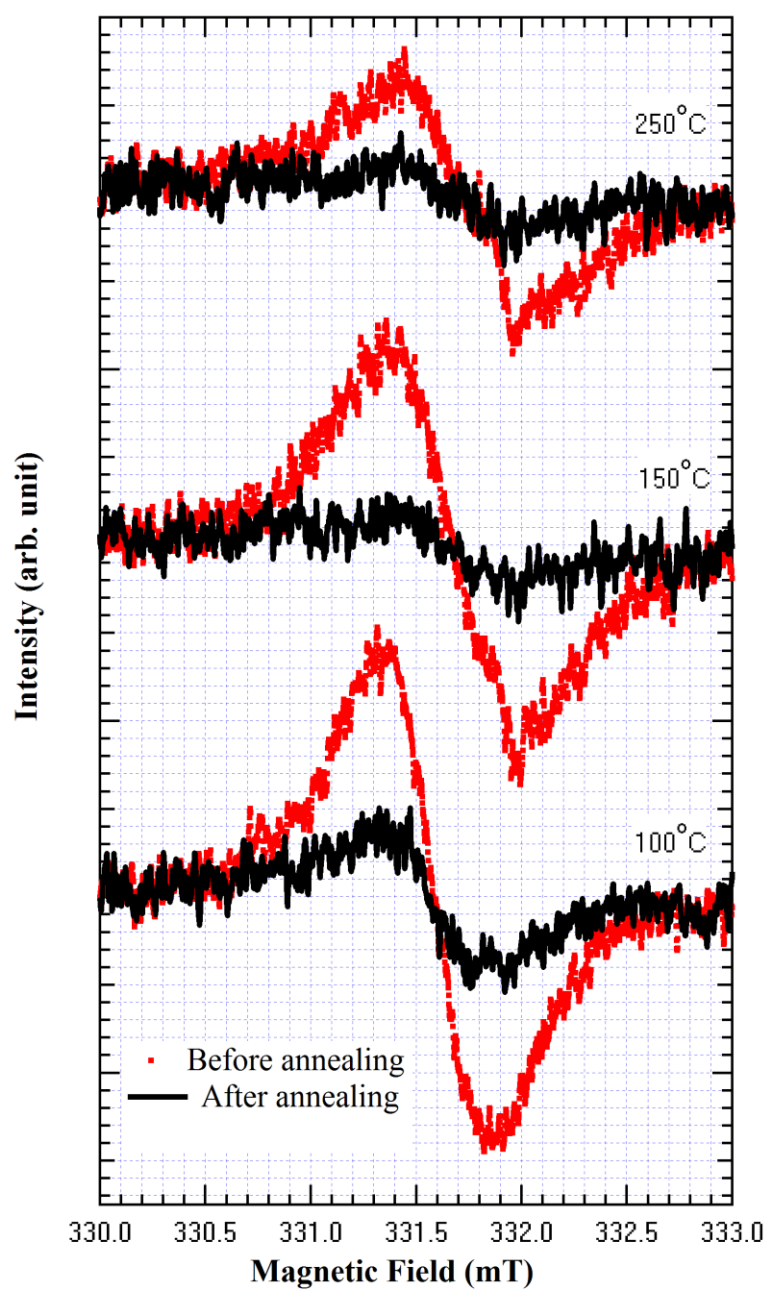


Figure 5

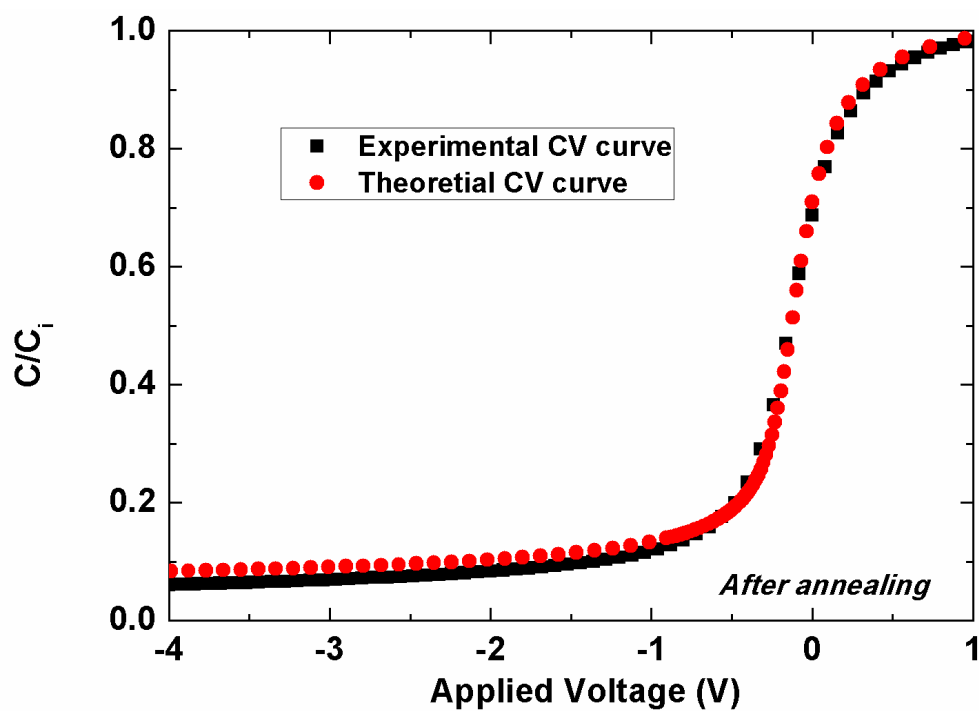
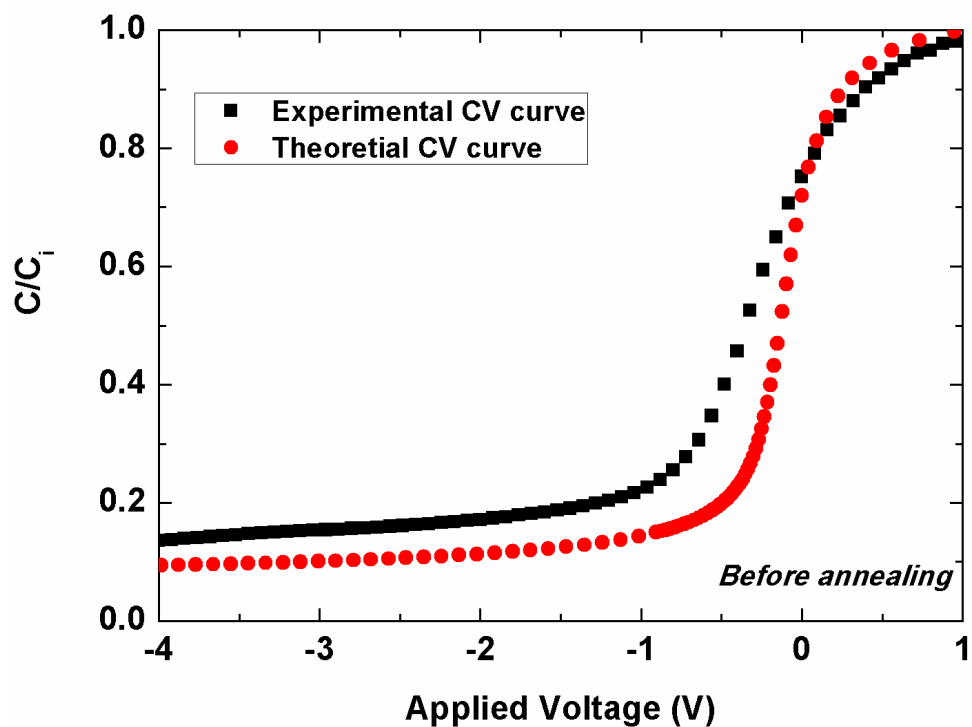


Figure 6

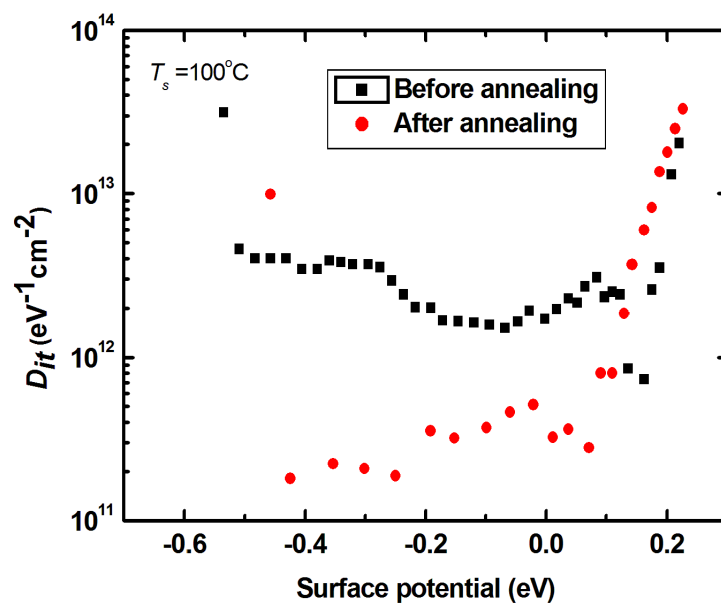
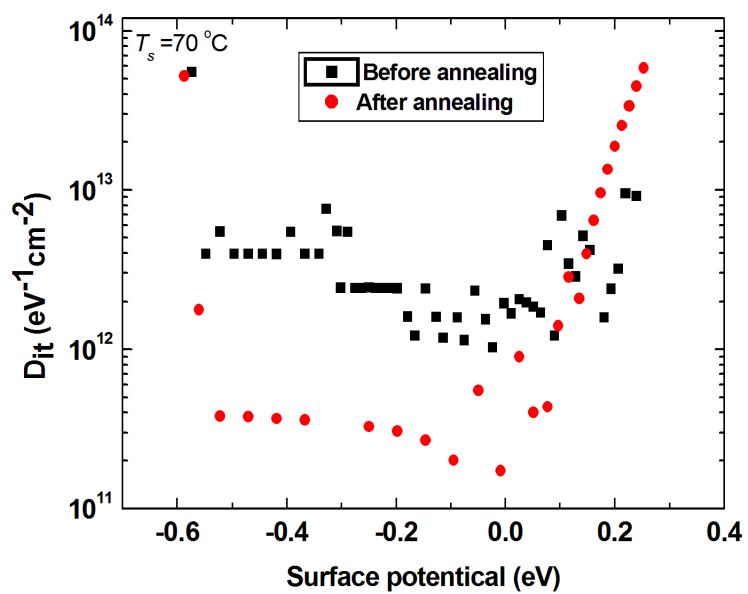


Figure 7

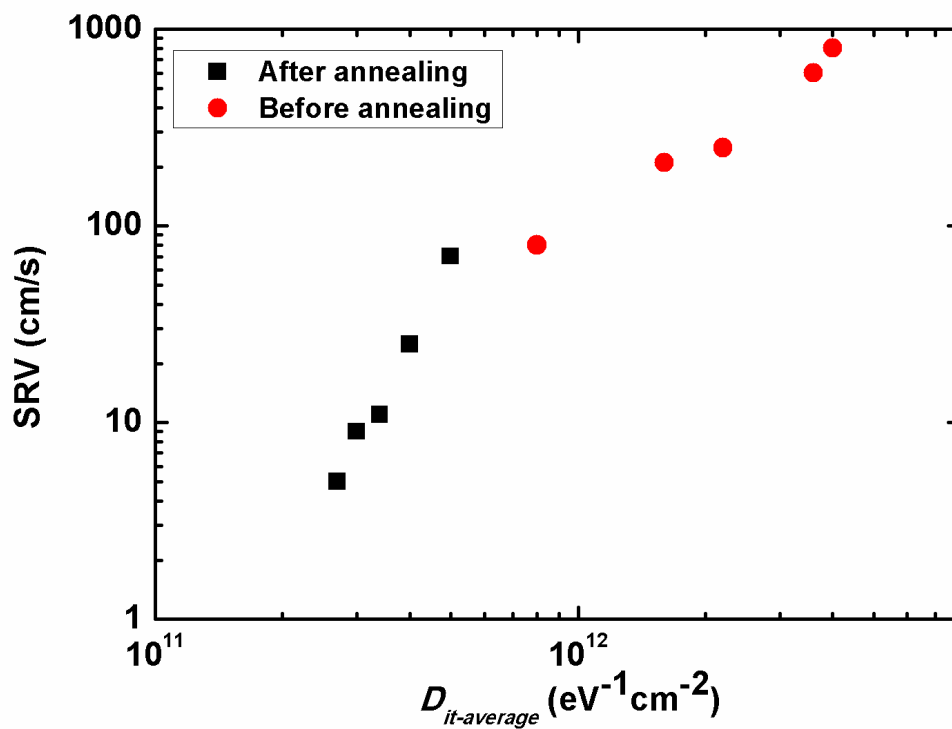


Figure 8

